

# Aggregation Limits Surface Expression of Homomeric GluA3 Receptors

**Coleman S., Hou Y., Willibald M., Semenov A., Moykkynen T. and Keinanen K.**

This is an author's accepted manuscript of an article published in the Journal of Biological Chemistry, first Published on February 24, 2016. The final definitive version is available online at:https://dx.doi.org/10.1074/jbc.M115.689125.

# Aggregation Limits Surface Expression of Homomeric GluA3 Receptors*

**Sarah K. Coleman, Ying Hou[§], Marina Willibald[§], Artur Semenov, Tommi Möykkynen, and Kari Keinänen**

From the Department of Biosciences (Division of Biochemistry and Biotechnology), University of Helsinki, Helsinki, Finland

*Running title: Aggregation of GluA3 subunits

To whom the correspondence should be addressed: Kari Keinänen, Department of Biosciences (Division of Biochemistry and Biotechnology), P.O. Box 56 (Viikinkaari 9), FI-00014 University of Helsinki, Helsinki, Finland. Tel: +358-50-3175026; E-mail: kari.keinanen@helsinki.fi

**Keywords**: AMPA receptors, assembly, ionotropic glutamate receptors, protein aggregation, protein folding, protein trafficking, surface expression

## ABSTRACT

**AMPA receptors are glutamate-gated cation channels assembled from GluA1-4 subunits and have properties that are strongly dependent on the subunit composition. The subunits have different propensities to form homomeric or various heteromeric receptors expressed on cell surface, but the underlying mechanisms are still poorly understood. Here, we examined the biochemical basis for the poor ability of GluA3 subunits to form homomeric receptors, linked previously to two amino acid residues, Y454 and R461, in its ligand-binding domain (LBD). Surface expression of GluA3 was improved by co-assembly with GluA2 but not with stargazin, a trafficking chaperone and modulator of AMPA receptors. The secretion efficiency of GluA2 and GluA3 LBDs paralleled the transport difference between the respective full-length receptors and was similarly dependent on Y454/R461, but not on LBD stability. In comparison to GluA2, GluA3 homomeric receptors showed a strong and Y454/R461-dependent tendency to aggregate both in the macroscopic scale measured as lower solubility in nonionic detergent and in the microscopic scale evident as the preponderance of hydrodynamically large structures in density gradient centrifugation and native gel electrophoresis. We conclude that the impaired surface expression of homomeric GluA3 receptors is caused by nonproductive assembly and aggregation to which LBD residues Y454 and R461 strongly contribute. This aggregation inhibits the entry of newly synthesized GluA3 receptors to the secretory pathway.**

α-Amino-3-hydroxy-5-methyl-4-isoxazolepropionic acid (AMPA) receptors are tetrameric ligand-gated ion channels which mediate fast excitatory neurotransmission in vertebrate brain (1,2). The functional properties of AMPA receptors, including channel kinetics, ion permeability, ligand pharmacology and regulation, are determined by the subunit composition. AMPA receptors are built from four subunit types (GluA1-4), each expressed as multiple alternatively spliced and/or RNA-edited variants. Studies with native and recombinant receptors indicate that receptor assembly is not random but strongly favors certain subunit combinations (3,4). The majority of native AMPA receptors are heteromers of edited GluA2 subunits with GluA1 or GluA3 subunits, forming channels which are impermeable to $Ca^{2+}$ and showing a linear current-voltage (I-V) relation (3,5,6). Minor native populations of homomeric AMPA receptors are formed by GluA1 or GluA4 subunits to produce inwardly rectifying and $Ca^{2+}$-permeable channels (7,8).

At present, the molecular logic underlying the formation and cellular processing of specific subunit assemblies in AMPA receptors is still poorly understood. The oligomerization is initiated by formation of dimers between N-terminal domains (NTD) of nascent receptor polypeptides in the endoplasmic reticulum (ER), followed by interactions involving the transmembrane segments and the ligand-binding domains (LBD) (9-11). The relative strength of

NTD contacts can partly explain the strong preference of certain subunits like GluA3 for heteromeric assembly, but also the LBD harbors important structural determinants which control the biogenesis of AMPA receptors in a subunit or subunit variant –dependent manner (12-14). In addition, auxiliary proteins, including transmembrane AMPA receptor-associated proteins (TARP) and cornichon homologs, associate with AMPA receptors already in the ER and, in principle, may influence the assembly process (9,15-17).

Recently, we demonstrated that two LBD residues, Y454 and R461, are responsible for the poor delivery of homomeric GluA3 receptors to cell surface both in the presence and absence of NTD (12). These residues are not directly engaged in glutamate binding nor in subunit interactions, and the reason why they inhibit the formation or transport of homomeric GluA3 to the cell surface is unclear. Here, we performed a comparative biochemical analysis of wild-type and mutated GluA2 and GluA3 receptors expressed in HEK293 cells. We found that GluA3 receptors exhibit aberrant, Y454/R461-dependent tendency to disturbed oligomerization and aggregation. Our findings suggest that subunit-dependent balance between transport-competent oligomers and higher-order abnormal assemblies contributes to the preferences of AMPA receptor subunits for homomeric or heteromeric expression.

## EXPERIMENTAL PROCEDURES

*DNA constructs* - All cDNAs encoding full-length AMPA receptor subunits or mutants thereof represented the rat AMPA receptor subunits; the flip/flop isoform is indicated in the text and figure legends; GluA2 is the edited (Q607R) form. All were expressed with an N-terminal signal sequence and tag from pcDNA3.1 (Stratagene) (12,13,18). Plasmids encoding human stargazin and rat GluN1 (NR1) were kind gifts from John L. Black III (Mayo Medical School, Rochester, MN), and Dr Rolf Sprengel (Max Planck Institute for Medical Research, Heidelberg, Germany), respectively. Mammalian expression constructs of GluA2 and GluA3 LBDs were built on pEGF-C1 (Clontech) by replacing the GFP encoding sequence by a cDNA expression cassette encoding an N-terminal signal peptide, Flag-epitope, requisite GluA sequences and C-terminal Myc-tag as described before for GluA4 (13). Bacterial expression constructs were created by PCR-based cloning and inserted into T7 promoter containing vector and a C-terminal 6xHis tag. The constructs were designed to correspond to AMPA receptor ligand-binding domains used for crystallization studies (19,20). All constructs were verified by restriction mapping and sequencing of PCR amplified regions.

*Antibodies* - For immunoblotting, the following antibodies were used: mouse monoclonal anti-Flag M1 (1 μg/ml; Sigma F-3040), anti-GAPDH (0.03 μg/ml; Sigma G-8795), and anti-GFP (1:1000; Sigma G6539), rabbit polyclonal anti-Myc (0.2 μg/ml; AbCam ab9106), anti-GluA2/3 IgG (1 μg/ml; Millipore #07-598), anti-GluN1 (0.2 μg/ml; Chemicon AB1516), anti-GRP78 (Sigma G-8918; 1:2000), and anti-stargazin serum (1:2000; Ref.13); horseradish peroxidase -conjugated anti-mouse (1:3000; NA931V) or anti-rabbit (1:3000; NA934V) IgGs, both from GE Healthcare, were used as secondary antibodies. For immunoprecipitation, mouse monoclonal anti-Flag M2 (2 μg/ml; Sigma F-3165) or anti-Myc (5 μg/ml; 9E10) were used.

*Cell culture and transfection* - HEK293 cells were cultured in DMEM supplemented with 10 % (v/v) fetal calf serum and penicillin-streptomycin, and transfected with appropriate plasmids by using calcium phosphate coprecipitation as previously described (21). For patch-clamp experiments, pEGFP1-C1 (Clontech) was co-transfected for the visualization of transfected cells. For some experiments, cells were incubated with tunicamycin (2 μg/ml; Sigma T-7765) for 24 hours prior to harvesting.

*Electrophysiology* – Whole-cell patch clamp recordings and analysis of glutamate-triggered currents in transfected cells were carried out as previously described (22). In brief, recordings from AMPA receptors expressing HEK293 cells were done at holding potential of -60 mV. L-glutamate was diluted in external recording solution containing 150 mM NaCl, 2.5 mM KCl, 2.5 mM $CaCl_2$, 1 mM $MgCl_2$, 10 mM glucose and 10 mM HEPES (pH 7.4; 320 mOsm) and applied to cells using a piezo driven applicator (Siskiyou Piezo Switcher; Siskiyou Corporation, OR, USA). Electrodes had resistance of 2-4 MΩ when filled with internal solution containing 140 mM CsCl, 2 mM $MgCl_2$, 10 mM EGTA and 10

mM HEPES (pH 7.2, 315 mOsm). Cells were lifted from the bottom of culture dish by the patch clamp pipette to facilitate the solution exchange. Each drug application was done twice and traces were averaged for analysis.

*Fluorescence microscopy* - Representative micrographs of GluA3-GFP expressing HEK293 cells were acquired via an EVOS fl digital inverted microscope (AMG, Life Technologies) with GFP LED light cube (570 nm excitation, 525 nm emission) and 20x objective.

*Biochemical Analyses* – Transfected cells were extracted in TNE buffer (50 mM Tris-HCl pH 7.4, 150 mM NaCl, 5 mM EDTA) containing 1% (w/v) Triton X-100, followed by ultracentrifugation at 100,000 x *g* for 1 h. Detergent-soluble and non-soluble receptor fractions were determined from the immunoreactivity present in the supernatant and in the pellet, respectively. They were quantitated as described below. Protein concentrations were determined by bicinchonic acid assay (Uptima, Interchim, France) using bovine serum albumin as standard. Immunoprecipitation, cell surface biotinylation and analysis of the secretion of ligand binding domain were performed as described previously (13,21,23).

Cell surface biotinylation was done as described (13). Briefly, transfected HEK293 cells were rinsed with PBS containing 1 mM $CaCl_2$, 0.5mM KCl, 2.5 mM $MgCl_2$, and incubated with EZ-Link sulfo-NHS-SS-Biotin (Pierce) at 0.5 mg/ml in the above buffer for 30 min at room temperature. Non-reacted reagent was removed by washing cells with the above buffer. Triton X-100 extracts were made as described above and subject to streptavidin-Sepharose precipitation (GE Healthcare). Immunoprecipitation was done as described (21). Briefly, Triton X-100 extracts of transfected cells were incubated with pre-washed Gamma-bind Sepharose (GE Healthcare) and appropriate antibody (at concentration detailed above) and mixed for 2 h at 4 °C.

Secretion of GluA2 and GluA3 LBDs was GluA S1S2 construct secretion was analyzed as described (23). Briefly, growth media was collected from transfected HEK293 cells 40 h after transfection, and 1 mM PMSF was added. Cell debris was pelleted by centrifugation (1500 g, 5 min, 4°C). The total cell extracts were prepared as above.

*Density gradient centrifugation* – Gradients were prepared by layering 10% (w/v) sucrose in TNE buffer containing 0.5 % Triton X-100 over 40% (w/v) sucrose solution (1:1 ratio) and incubating horizontally for 75 min at room temperature. Thus prepared gradients were stored vertically at 4 °C until use. Transfected HEK293 cell extracts (300 µl) were layered on top of the gradients which were run in pairs in ultracentifuge with Sw-55Ti rotor (Beckman-Coulter) at 175,000 x *g* for 16 h at +4 °C. Fractions (200 µl) were collected from the bottom of centrifuge tube by using peristaltic pump (Pharmacia Biotech P-1).

*Gel electrophoresis analysis* – Samples were run on either Lonza 4-12% or Bio-Rad 4-15% TGX Criterion gradient gels for both denaturing (SDS) or Blue Native (BN)-polyacrylamide gel electrophoresis (PAGE). For SDS-PAGE samples were prepared in Laemmli sample buffer (with final concentration of 60 mM Tris-Cl pH 6.8, 2% SDS, 10% glycerol, 5% β-mercaptoethanol, 12.5 mM EDTA 0.01% bromophenol blue). BN-PAGE was run according to the protocol of Gill et al. (24) and samples were prepared in native loading buffer (with final concentration of 60 mM Tris-Cl pH 6.8, 10% glycerol, 0.01% bromophenol blue); molecular standards were indicated by Native Mark (Novex, Life Technologies). Following gel separation, proteins were transferred onto Hybond membrane (GE Healthcare) and immunoblotted. The samples used for BN-PAGE were obtained from the sucrose density gradients with the exception of the analysis of crude cell extracts. In the latter case, Triton X-100 extracts prepared from transfected cells were cleared by centrifugation at 12,000 x *g* for 20 min, mixed with native loading buffer and used for electrophoresis.

*Immunoblotting and analysis* – For immunoblotting, Clarity™ Western ECL substrate (Bio-Rad, 170-5061) was used. ECL signal was detected and measured either by ChemiDoc XRS system and Quantity One software (BioRad) or by BioSpectrum 810 and VisionWorksLS software (Ultra-Violet Products Ltd, UK). The pixel density of the immunoreactive bands was obtained from the longest possible exposure prior to saturation of signal. If required the relative expression levels were normalised to a control, as defined in the respective figure legend. For determination of percentage of oligomeric state following BN-

PAGE, the signal was summed from boxes corresponding to aggregate, tetramer, dimer and monomer for all fractions run (see Figure 7A middle panel). An equivalent box for background only was also measured, if this corresponded to 5 % or more of total signal the experiment was discarded.

*Bacterial protein expression and purification* – 6xHis-tagged proteins were expressed and purified according to standard procedures as described previously (25) with the following modifications; the plasmids containing wild type or point-mutated GluA2i S1S2 and GluA3i S1S2 segments were transformed into *E. coli* Origami (DE3)pLysS for protein expression. The first round of purification from *E. coli* lysates was made via Ni-NTA agarose (Qiagen) against the 6xHis-tag. The proteins eluted from Ni-NTA agarose were dialyzed against 20 mM Tris-HCl, pH 8.0 buffer and then loaded on to a DEAE column (DEAE-Sepharose CL-6B, Pharmacia). Following washing proteins were eluted with 20 mM Tris-HCl pH 8.0 buffer containing 0.1 M NaCl. All purified proteins were concentrated by centrifugal devices (microsep 30K, Pall) to approximately 2 mg/ml and stored in elution buffer solution at 4$^{o}$C.

*Chemical denaturation* – Aliquots of bacterially expressed and purified GluA2 or GluA3 LBD proteins were incubated with increasing concentrations of urea (0-8 M) in the presence or absence of 10 mM L-glutamate. Intrinsic fluorescence at 300-450 nm region produced by excitation at 295 ± 5 nm was measured in quartz cuvettes (Hellma) using a FluoroMax-4 spectrofluorometer (Horiba Scientific), and analyzed by Origin 7.5 software. For calculation of the urea denaturation curves peak emission intensities at 325 nm and 327 nm were used for for GluA2 and GluA3 LBDs, respectively. Fluorescence intensity was plotted against urea concentration and individually best-fit with sigmoidal dose-response (variable slope and no constraints) model in in GraphPad Prism v4 (GraphPad Software Ltd).

*Circular dichroism (CD) spectroscopy* – For CD spectroscopy protein samples were dialyzed overnight against sodium phosphate buffer (50 mM sodium phosphate pH 7.4), followed by centrifugation (5 min, 13,000 rpm, 4°C). Thermal stability of the GluA2i, GluA3i and GluA3i (Y454A/R461G) LBDs was monitored by CD-spectroscopy using a Jasco J-720 spectropolarimeter. Thermal denaturation scans were recorded using a 0.1 cm cuvette, wavelength 195 nm, a temperature range from 20°C to 70°C with temperature steps of 0.1°C. The protein concentration was 0.2 mg/ml. CD-spectra were measured in presence and absence of L-Glutamate at 1 mM for GluA3i and GluA3i (Y454A/R461G) and 0.5 mM for GluA2i. Data was compiled in Excel (Microsoft Office 2007). The spectra were plotted and Tm calculated with GraphPad Prism v4 (GraphPad Software Ltd).

*Statistical Analysis* – Data are presented as mean ± SEM, unless otherwise stated and described, where n is the number of independent experiments. Analysis was by Student's *t*-test or by one or two-way ANOVA followed by Bonferroni's multiple comparison test or by Dunnett's multiple comparison test to control. Statistical significance of *p* values was indicated by asterisks as follows: * $p < 0.05$; ** $p < 0.01$; *** $p < 0.001$. All statistical analyses were done by using GraphPad Prism. Analysis of desensitization kinetics of patch clamp recordings were done by Clampfit 10.2 software (Molecular devices, Sunnyvale CA, USA) using single exponential fit paradigm.

## RESULTS

***Surface expression of GluA3 is rescued by co-assembly with GluA2 but not by association with stargazin.*** Previously, we showed that co-expression with GluA2-flip (GluA2i) promotes the surface expression of the otherwise mostly intracellularly retained GluA3i in transfected HEK293 cells (12). We now analyzed the ability of GluA2 isoforms, flip and flop (GluA2o) and of the GluA2i point mutant GluA2i A451Y/G458R (GluA2i AG/YR) to promote GluA3i surface expression as determined by biotinylation assay. Biotinylation with the cell-impermeant biotin derivative interferes with immunoreactivity of extracellular epitopes so a GFP tag was introduced to the C-terminus of the receptor polypeptide. This C-terminal fusion does not alter the basic trafficking of GluA2 and GluA3 as GluA2i-GFP showed significant surface expression, whereas only a minor fraction of Glu3i-GFP was present on the plasma membrane (Fig. 1*A*). Thus, GluA3i-GFP was expressed in HEK293 cells together with the Flag-tagged test constructs GluA3i (control),

GluA2i, GluA2o, or GluA2i(AG/YR). After surface biotinylation and streptavidin pulldown, GluA3i-GFP was visualized by immunoblotting (Fig. 1, *B* and *C*). Consistent with earlier findings, heteromeric assembly improved the surface expression of the GluA3i: in the presence of GluA2i, plasma membrane levels of GluA3i-GFP increased six-fold. Co-expression with the flop isoform of GluA2 and with the AG/YR double mutants which carry the two residues responsible for the intracellular retention of GluA3, did not the increase surface expression of GluA3i-GFP in a statistically significant manner (Fig. 1*C*). In order to determine whether GluA3 displays significant preference for heteromeric over homomeric assembly, N-terminally tagged GluA2i and GluA3i were expressed with a differently tagged version of the same or the other subunit, and subjected to immunoprecipitation. Flag-tagged GluA3i was co-immunoprecipitated with myc-tagged GluA3i or GluA2i and vice-versa to similar extent. Thus, suggesting that under the experimental conditions of transient expression in HEK293 cells GluA3 has no significant preference for heteromeric assembly (Fig. 1*D*).

In addition to co-assembly, association with auxiliary proteins is known to promote surface expression of AMPA receptors. Therefore, we studied whether co-expression with stargazin (a prototype member of transmembrane AMPA receptor regulatory proteins) would promote the trafficking of GluA3 to the plasma membrane. Previously, we have shown that stargazin rescues the otherwise poor surface expression of the flop variants of GluA1 and GluA4 homomers (13). However, despite strong expression and surface location of stargazin no significant improvement was seen for GluA3 (Fig. 2, *A* and *B*). Due to this unexpected result, it was important to verify the association of stargazin with GluA3. Co-immunoprecipitation experiments did not show statistically significant difference in stargazin association between GluA3 and GluA2 (Fig. 2*C*). Whole cell patch clamp electrophysiology on transfected HEK293 cells did not show a statistically significant increase in the maximal whole-cell currents in the presence of stargazin, (Fig. 2*D*). However, when stargazin was co-expressed the desensitization of glutamate responses was significantly slower: time-constants ($\tau_{des}$ values) for the onset of desensitization were 10.48 ms ± 1.11 for GluA3+Stg and 4.50 ms ± 0.38 GluA3 for GluA3 alone, indicating functional association of stargazin with GluA3 (Fig. 2*E*).

***Differences in LBD stability do not explain the poor trafficking of GluA3.*** Ligand-binding domains of GluA2 and GluA3, expressed as soluble secretable fusion proteins, reproduce the trafficking difference between the subunits (12). It is not clear, however, whether the underlying mechanisms are shared. In order to resolve this question we analyzed whether the two amino acid differences in LBD, which explain the differing surface expression levels of intact GluA2 and GluA3, can similarly affect the secretion of LBDs. Epitope-tagged LBD constructs were expressed in HEK293 cells and LBD protein levels were determined in the cells and culture medium by Western blotting (Fig. 3, *A* and *B*). In agreement with earlier results, wild-type GluA2 LBD was well secreted from the cells, whereas GluA3 LBD was not. Importantly, the double mutants GluA3(YR/AG) and GluA2(AG/YR) reversed the behavior and showed secretion patterns typical for the other subunit: GluA3(YR/AG) LBD was secreted efficiently to the culture medium, wheras GluA2(AG/YR) LBD was largely retained in the cells (Fig. 3, *B* and *C*). All LBD constructs were equally well expressed within the cells (Fig. 3B, left panels).

The above results suggest that similar mechanisms contribute to the transport defects of full-length GluA3 and GluA3 LBD. One obvious possibility is that GluA3 LBD is less stable and because of local unfolding GluA3 or GluA3 LBD would not be able to pass the quality control of the secretory pathway. To produce sufficient protein for the measurement of the conformational stability, we engineered the LBD constructs for expression in *E. coli*. The LBDs contain one essential disulfide bond so *E.coli* strain Origami, which harbors oxidizing cytosol, was used as the expression host. Initial attempts to express LBDs which had an overall design as shown in Figure 3*A*, but lacking the signal peptide, failed to produce any significant levels of protein. Therefore, the LBDs were redesigned to correspond to the GluA2 S1S2J construct (19) that has been used in a similar expression system to produce GluA2 and GluA3 LBDs for crystallization (20) (Fig. 4*A*). This approach led to successful expression of both LBDs as soluble

proteins (although GluA3 yields were consistently lower) and the proteins were purified by using metal-chelation affinity chromatography. Stability was assessed by measuring the intrinsic tryptophan fluorescence in increasing concentrations of urea in the presence and absence of L-glutamate (10 mM). Typical plots of fluorescence intensity against urea concentration are shown in Figure 4*B*; they were sigmoidal and showed a marked shift to the right (to higher urea concentrations) in the presence of glutamate, indicative of co-operative unfolding and stabilization by glutamate (Fig. 4*B*): The $EC_{50}$ values for urea-induced unfolding are given (Fig. 4*C* and Table 1). Interestingly, GluA3 appeared more stable than GluA2, effectively ruling out poor folding of GluA3 LBD as an explanatory factor of the transport defect. To verify the results from chemically-induced unfolding we analyzed the thermostability of GluA2 and GluA3 LBDs by circular dichroism (CD) spectroscopy. Consistent with the results from chemically-induced denaturation the GluA3 LBD was more stable for thermally triggered unfolding (Fig. 4*D*). The presence of L-glutamate provided substantial stabilization for both LBDs, the $T_m$ values increased by over ten degrees Celsius for both GluA2 and GluA3 LBDs (Fig. 4*D* and Table 1). Interestingly, the thermostability of the LBD mutant GluA3 (YR/AG), which reverses the trafficking phenotype to GluA2-like, showed similar stability as the GluA3 wild-type both in presence and absence of L-Glutamate (Fig. 4*D* and Table 1. The results indicate that the differences between GluA2 and GluA3 in LBD stability and in the transport can be separated. Thus, stability and transport competency are likely independent from each other.

***Homomeric GluA3 receptors have a tendency for abnormal oligomerization and aggregation.*** In order to identify possible gross differences in the biochemical properties of GluA2 and GluA3, we determined the detergent-solubility of homomeric GluA2 and GluA3 receptors expressed in HEK293 cells. For this purpose, Triton X-100 –soluble and insoluble fractions were separated by ultracentrifugation and analyzed by SDS-PAGE and immunoblotting (Fig. 5*A*). There was a substantial difference between the subunits: 70 % of GluA2 protein (determined by using anti-Flag antibody) was solubilized by Triton X-100, whereas the fraction of detergent-soluble GluA3 was only half of that (Fig. 5, *A* and *B*). If the poor solubility of GluA3i is due to aggregation, it is possible that it could increase aggregation of other proteins coexpressed with it. To test this, we studied the detergent solubility of the GluN1 subunit of the NMDA receptor when coexpressed with either GluA3i or with GFP. Expression with GluA3i led to a significant increase in the amount of insoluble GluN1 (Fig. 5, *C* and *D*), supporting aggregation as an explanation for the poor detergent-solubility of GluA3i homomers. To find out whether the detergent-solubility is related to the trafficking phenotypes, the detergent-soluble fractions of wild-type and the reciprocal double mutated GluA2 and GluA3 flip and flop receptors were analyzed in parallel and normalized to GAPDH (serving as a loading standard for cellular protein). For both flip (Fig. 5, *E* and *F*) and flop (Fig. 5, *G* and *H*) isoforms, the point mutations completely reversed the solubility properties of the parental receptors; GluA3 YR/AG behaved like wild-type GluA2 and GluA2 AG/YR showing GluA3-like low detergent-solubility. Next, we examined the effects of expression of GluA2i and GluA3i on GRP78, an indicator of stress in the endoplasmic reticulum. In comparison to mock-transfected cells, the amount of GRP78 protein was slightly elevated in cells expressing GluA2i and GluA3i, but there was not difference between the subunits (Fig. 5*I*). In contrast, GRP78 level was strongly increased in tunicamycin-treated cells (2 µg/ml; 24 hours), used as a positive control. Anti-Flag immunoprecipitations showed that GRP78 is associated with both subunits to the same extent (Fig. 5*J*).

The above-described results suggest that while the crucial difference between GluA2 and GluA3 homomeric receptors is strictly related to specific LBD residues, the mechanistic explanation for the different transport competences of GluA2 and GluA3 receptors does not lie in the primary folding of the LBD, but more likely in the solution behavior of the cognate receptors. This prompted us to analyze the oligomeric state of GluA2, GluA3 and GluA3 (YR/AG) receptors by using fractionation of detergent-soluble receptors in sucrose density gradient centrifugation. Anti-Flag immunoblots of sucrose gradient fractions showed remarkable differences between the receptor variants (Fig. 6*A*). The majority of GluA3 110-kDa signal was associated with the higher density

sucrose fractions with a broad peak (P1) at fractions 5-7 with substantial immunoreactivity also present at the bottom of the gradient, likely representing aggregation (Fig. 6*B*). A minor population of GluA3 sedimented at a lower speed forming a distinct peak at fractions 13-14 (P2). In contrast, most of GluA2 sedimented in a uniform manner producing a peak coinciding with P2. A minor fraction of GluA2 was present in the higher density fractions. The mutant GluA3 YR/AG showed intermediate behavior distributing equally between the two peaks P1 and P2, but was also present in the fractions between these peaks (Fig. 6*B*). In addition to the 110-kDa receptor subunit monomer band a diffuse ~250-kDa band was prominently present in the peak fractions of GluA2 and GluA3, in amounts which correlated roughly with the monomer band. This had been noticed previously and assigned to SDS-resistant assembly intermediates (26). Additionally, with GluA3 samples, the densest fractions at the bottom of tube produced further intense diffuse smear-like immunoreactivity at very high molecular weight region (Fig. 6*A*). Due to this complex distribution of immunoreactivity we quantitated the immunoreactivity separately for the 110-kDa band (Fig. 6*B*) and for the entire sample lane (Fig. 6*C*). Inclusion of the diffuse immunostaining at ≥ 250-kDa region did not significantly affect the overall result, but blurred the P1 peak of GluA3 protein because of the large amount of aggregates in the bottom fractions (Fig. 6*C*).

In order to determine the major oligomeric state(s) of the receptor in P1 and P2, we subjected a sample of every other sucrose gradient fraction to BN-PAGE followed by immunoblotting. The samples were separated to four populations by rate of migration in the gel, which were assigned as aggregates (Ag), tetramers (T), dimers (D) and monomers (M) (Fig. 7*A*) as based on previous studies (24,27). The highest-density sucrose fractions resolved into diffuse large-sized aggregates, whereas P1 and P2 peaks best coincided with the tetramer and dimer populations. Monomeric form was only (occasionally) seen in the post-P2 fractions of GluA2 protein (Fig. 7*A*). Quantitative analysis of the respective band intensities from five independent experiments revealed the strong presence of aggregates in GluA3 and dimers in GluA2 as the most striking differences between the subunits (Fig. 7*B*). Again, the double mutant GluA3 YR/AG showed intermediate behavior. Tetramers accounted for 25-28 % of the total immunoreactivity in all three receptor variants. The ratio of dimers-to-tetramers was about 0.40 for GluA3 and 2.0 for GluA2 (Fig. 7*C*), the predominance of dimers in GluA2 being in agreement with previous studies of GluA2 biogenesis (26, 27). We also analyzed the Triton X-100 –extracts directly by BN-PAGE, without prior fractionation in sucrose gradient. The results confirm the strong presence of the dimeric species in wild-type GluA2i and its virtual absence in GluA3i. Moreover, the double mutants GluA2i AG/YR and GluA3i YR/AG showed banding patterns which were intermediate of their parental wild-type subunits (Fig. 7*D*).

The sucrose density gradient fractionation and BN-PAGE analysis indicate that GluA3 receptors have a much stronger tendency to form tetramers and larger oligomers/aggregates than GluA2 and this difference is largely but not totally eliminated by the YR/AG double mutation.

## DISCUSSION

Native GluA3 subunits are predominantly associated with GluA2 (6,28) and coexpression with GluA2 (12; this study) rescues the otherwise poor surface expression of recombinant GluA3 subunits (12,29), suggesting that GluA3 is an "obligatory heteromeric" subunit. Two amino acid residues, Y454 and R461, were previously identified as critical determinants of the poor surface expression of homomeric GluA3 receptors (12). Substituting the residues with their GluA2 counterparts, alanine and glycine respectively, rescues the surface expression of GluA3 homomers to GluA2 levels, and conversely, their incorporation to GluA2 leads to dramatic decrease in the transport to cell surface (12). The location of these residues in the ligand-binding domain but outside of known subunit interfaces and the ligand binding cleft makes their striking effect on receptor transport enigmatic. Here, we wished to elucidate the biochemical mechanisms responsible for the inefficient expression of homomeric GluA3 receptors on the plasma membrane by examining the differences in molecular properties between GluA2 and GluA3 receptors and their dependence on the YR/AG residues.

Our analysis of full-length receptors identified detergent-solubility as a biochemical

property which clearly distinguished between GluA2 and GluA3 and was strongly dependent on the YR/AG residues. The majority of GluA2 expressed in HEK293 cells was soluble in Triton X-100, whereas most of immunoreactive GluA3 appeared as insoluble aggregates. Double mutations at YR/AG positions shifted the solubility of GluA2 or GluA3 towards the other subunit, indicating that Y454 and R461 promote aggregation. To find out if this is caused by poor folding or instability of GluA3 LBD, we expressed wild-type and mutated GluA2 and GluA3 LBDs as soluble fusion proteins. The secretion efficiencies of GluA2 and GluA3 LBDs in HEK293 cells closely mimicked the transport phenotypes of the cognate membrane-bound receptors, and were completely reversed by mutations at the YR/AG residues. Spectroscopic analysis of the unfolding of purified LBDs, purified from *E.coli* expression, yielded classical cooperative unfolding curves for both GluA2 and GluA3. Unexpectedly, GluA3 LBD appeared more stable than GluA2 against both urea-induced and thermal denaturation, but this effect was unrelated to the trafficking difference as the GluA3 YR/AG double mutant showed similar stability to wild-type GluA3. These findings suggest that the aggregation-promoting effect of Y454/R461 residues is not caused by unstable fold of GluA3 LBD. Of note, the occurrence of thermal denaturation of ligand-free LBDs at or near physiological temperature, together with the strong stabilizing effect by glutamate, are consistent with the emerging concept that glutamate in the ER acts as a physiological chaperone in AMPA receptor folding (23,24,30-32).

Analysis of the detergent-soluble receptors, assumed to represent the properly folded protein, by sucrose density gradient centrifugation and blue native gel electrophoresis revealed differences in the oligomeric status of GluA2 and GluA3 proteins. Major immunoreactive peaks from sedimentation in density gradients resolved in higher oligomers/microaggregates, tetramers and dimers. Consistent with aggregation in the macroscopic scale, over half of immunoreactive GluA3 existed as microaggregates or complexes larger than tetramers. GluA2 and GluA3 preparations contained tetramers at similar relative amounts, but the proportion of dimers was much higher for GluA2, in agreement with an earlier study (27). The double mutation YR-to-AG shifted the hydrodynamic behavior and dimer-to-tetramer ratio of GluA3 towards GluA2, albeit not completely. The lower dimer-to-tetramer ratio (0.4:1) suggests that GluA3 tetramers are more stable/less dynamic than those of GluA2 (2:1). Considering this fact with the failure of stargazin, which associates selectively with tetrameric AMPA receptors in the ER (33,34), to significantly promote GluA3 surface expression, we speculate that the (majority of) GluA3 tetramers do not represent the native conformation but some incompletely matured intermediate.

Our study shows that homomeric GluA3 receptors are prone to aggregation at both molecular and macroscopic levels, and that this tendency is strongly linked to the two residues which determine the intracellular retention of GluA3 homomers. In an attempt to provide a mechanistic explanation for these findings, we present a tentative model (Fig. 8) which accommodates our experimental results with the body of current research literature on AMPA receptor assembly (for reviews, see Refs. 35-38). The crystal structure of GluA2 tetramers shows that the LBDs and NTDs are organized as pairs of dimers, one subunit in each pair occupying a proximal and the other a distal position around the central axis, whereas the membrane-associated regions are arranged around the ion channel in a four-fold symmetrical fashion (10). Based on the GluA2 tetramer structure, the critical GluA3 residues Y454 and R461 would point outwards from the tetramer in the proximal LBDs and inwards in the distal LBDs (12). Heteromeric AMPA receptors are believed to have a 2:2 stoichiometry with the subunits adopting an alternating arrangement ("1-2-1-2"; Refs. 3,39), which in the case of GluA2/3 is ensured by preferred formation of NTD heterodimers (11,35,40). Thus, depending on whether the GluA3 subunits would favor the proximal or the distal positions in the LBD layer, the critical residues would be either exposed on the tetramer´s outer surface or masked inside. The rescue of plasma membrane expression and decrease of GluA3 aggregation would then arise from preferential adaptation of GluA3 LBDs of one of the two alternative orientations upon coassembly with GluA2. Whether the outer or inner orientation is detrimental to proper maturation and surface

expression is presently unclear. However, we favor a scanario in which the outward orientation of Y454/R461 residues would lead to aggregation through lateral interactions, as we suggested earlier (12) based on the location of homologous GluA2 residues at an intermolecular interface present in an LBD crystal structure (19,20). Therefore, we propose that upon heteromeric assembly with GluA2, GluA3 LBDs would strongly favor the distal positions (as in heteromer 2; Fig. 8B). In contrast, in GluA3 homomers (and in the unfavored heteromer 1-like GluA2/3 receptors), the exposed Y454/R461 residues would drive the formation of higher oligomers, impeding maturation and transport to cell surface (Fig. 8*C*). Similarly, the poor secretion of GluA3 LBD would be caused by a tendency to form head-to-tail intermolecular contacts, which may interfere with efficient secretion. The other scenario which gives the critical role to the inwardly oriented residues, is more difficult to reconcile with the LBD data.

To summarize, one of the two orientations of GluA3 residues Y454 and R461 promotes aggregation and formation of transport-incompetent tetramers, resulting in intracellular retention of homomeric GluA3 receptors. Coassembly with GluA2 leads to elimination of the deleterious orientation allowing the forward trafficking of GluA2/3 heteromers to the cell surface. In conclusion, our results demonstrate that propensity to aggregate can explain subunit-dependent differences in surface expression of AMPA receptors. Interestingly, the critical determinant for the poor surface transport of homomeric GluA1 and GluA4 flop receptors, a single Leu/Val residue, is positioned quite close to the Y454 and R461 studied in GluR3 (13, 20). Future studies will reveal whether the mechanisms identified here for GluA3 will also apply to the poor trafficking of flop variants.

**Conflict of interest:** The authors declare that they have no conflicts of interest with the contents of this article.

**Authors Contributions:** S.K.C. designed and carried out most experiments and wrote the manuscript. Y.H. and M.W carried out experiments with bacterially expressed protein. A.S. helped optimize bacterial expression and protein purification and set up spectroscopy experiments. T.M. carried out electrophysiological recordings and their analyses. K.K. supervised the project, designed experiments and wrote the manuscript. All authors reviewed the results and approved the final version of the manuscript.

**REFERENCES**


1. Palmer, C.L., Cotton, L., and Henley, J.M. (2005) The molecular pharmacology and cell biology of alpha-amino-3-hydroxy-5-methyl-4-isoxazolepropionic acid receptors. *Pharmacol. Rev.* **57,** 253-277
2. Traynelis, S.F., Wollmuth, L.P., McBain, C.J., Menniti, F.S., Vance, K.M., Ogden, K.K., Hansen, K.B., Yuan, H., Myers, S.J., and Dingledine, R. (2010) Glutamate receptor ion channels: structure, regulation, and function. *Pharmacol. Rev.* **62,** 405-496
3. Mansour, M., Nagarajan, N., Nehring, R.B., Clements, J.D., and Rosenmund, C. (2001) Heteromeric AMPA receptors assemble with a preferred subunit stoichiometry and spatial arrangement. *Neuron.* **32,** 841-853
4. Greger, I.H., and Esteban, J.A. (2007) AMPA receptor biogenesis and trafficking. *Curr. Opin. Neurobiol.* **17,** 289-297
5. Wenthold, R.J., Petralia, R.S., Blahos, J.,II, and Niedzielski, A.S. (1996) Evidence for multiple AMPA receptor complexes in hippocampal CA1/CA2 neurons. *J. Neurosci.* **16,** 1982-1989
6. Lu, W., Shi, Y., Jackson, A.C., Bjorgan, K., During, M.J., Sprengel, R., Seeburg, P.H., and Nicoll, R.A. (2009) Subunit composition of synaptic AMPA receptors revealed by a single-cell genetic approach. *Neuron.* **62,** 254-268
7. Cull-Candy, S., Kelly, L., and Farrant, M. (2006) Regulation of Ca2+-permeable AMPA receptors: synaptic plasticity and beyond. *Curr. Opin. Neurobiol.* **16,** 288-297

8. Isaac, J.T., Ashby, M., and McBain, C.J. (2007) The role of the GluR2 subunit in AMPA receptor function and synaptic plasticity. *Neuron.* **54,** 859-871
9. Shanks, N.F., Maruo, T., Farina, A.N., Ellisman, M.H., and Nakagawa, T. (2010) Contribution of the global subunit structure and stargazin on the maturation of AMPA receptors. *J. Neurosci.* **30,** 2728-2740
10. Sobolevsky, A.I., Rosconi, M.P., and Gouaux, E. (2009) X-ray structure, symmetry and mechanism of an AMPA-subtype glutamate receptor. *Nature.* **462,** 745-756
11. Rossmann, M., Sukumaran, M., Penn, A.C., Veprintsev, D.B., Babu, M.M., and Greger, I.H. (2011) Subunit-selective N-terminal domain associations organize the formation of AMPA receptor heteromers. *EMBO J.* **30,** 959-971
12. Coleman, S.K., Moykkynen, T., Hinkkuri, S., Vaahtera, L., Korpi, E.R., Pentikainen, O.T., and Keinanen, K. (2010) Ligand-binding Domain Determines Endoplasmic Reticulum Exit of AMPA Receptors. *J. Biol. Chem.* **285,** 36032-36039
13. Coleman, S.K., Moykkynen, T., Cai, C., von Ossowski, L., Kuismanen, E., Korpi, E.R., and Keinanen, K. (2006) Isoform-specific early trafficking of AMPA receptor flip and flop variants. *J. Neurosci.* **26,** 11220-11229
14. Penn, A.C., Williams, S.R., and Greger, I.H. (2008) Gating motions underlie AMPA receptor secretion from the endoplasmic reticulum. *EMBO J.* **27,** 3056-3068
15. Vandenberghe, W., Nicoll, R.A., and Bredt, D.S. (2005) Stargazin is an AMPA receptor auxiliary subunit. *Proc. Natl. Acad. Sci. U. S. A.* **102,** 485-490
16. Kim, K.S., Yan, D., and Tomita, S. (2010) Assembly and stoichiometry of the AMPA receptor and transmembrane AMPA receptor regulatory protein complex. *J. Neurosci.* **30,** 1064-1072
17. Gill, M.B., Kato, A.S., Roberts, M.F., Yu, H., Wang, H., Tomita, S., and Bredt, D.S. (2011) Cornichon-2 modulates AMPA receptor-transmembrane AMPA receptor regulatory protein assembly to dictate gating and pharmacology. *J. Neurosci.* **31,** 6928-6938
18. Pasternack, A., Coleman, S.K., Jouppila, A., Mottershead, D.G., Lindfors, M., Pasternack, M., and Keinanen, K. (2002) Alpha-amino-3-hydroxy-5-methyl-4-isoxazolepropionic acid (AMPA) receptor channels lacking the N-terminal domain. *J. Biol. Chem.* **277,** 49662-49667
19. Armstrong, N., and Gouaux, E. (2000) Mechanisms for activation and antagonism of an AMPA-sensitive glutamate receptor: crystal structures of the GluR2 ligand binding core. *Neuron.* **28,** 165-181
20. Ahmed, A.H., Wang, Q., Sondermann, H., and Oswald, R.E. (2009) Structure of the S1S2 glutamate binding domain of GluR3. *Proteins.* **75,** 628-637
21. Coleman, S.K., Cai, C., Mottershead, D.G., Haapalahti, J.P., and Keinanen, K. (2003) Surface expression of GluR-D AMPA receptor is dependent on an interaction between its C-terminal domain and a 4.1 protein. *J. Neurosci.* **23,** 798-806
22. Moykkynen, T., Coleman, S.K., Semenov, A., and Keinanen, K. (2014) The N-terminal domain modulates alpha-amino-3-hydroxy-5-methyl-4-isoxazolepropionic acid (AMPA) receptor desensitization. *J. Biol. Chem.* **289,** 13197-13205
23. Coleman, S.K., Moykkynen, T., Jouppila, A., Koskelainen, S., Rivera, C., Korpi, E.R., and Keinanen, K. (2009) Agonist occupancy is essential for forward trafficking of AMPA receptors. *J. Neurosci.* **29,** 303-312
24. Gill, M.B., Vivithanaporn, P., and Swanson, G.T. (2009) Glutamate binding and conformational flexibility of ligand-binding domains are critical early determinants of efficient kainate receptor biogenesis. *J. Biol. Chem.* **284,** 14503-14512
25. Cai, C., Coleman, S.K., Niemi, K., and Keinanen, K. (2002) Selective binding of synapse-associated protein 97 to GluR-A alpha-amino-5-hydroxy-3-methyl-4-isoxazole propionate receptor subunit is determined by a novel sequence motif. *J. Biol. Chem.* **277,** 31484-31490
26. Greger, I.H., Akamine, P., Khatri, L., and Ziff, E.B. (2006) Developmentally regulated, combinatorial RNA processing modulates AMPA receptor biogenesis. *Neuron.* **51,** 85-97
27. Greger, I.H., Khatri, L., Kong, X., and Ziff, E.B. (2003) AMPA receptor tetramerization is mediated by Q/R editing. *Neuron.* **40,** 763-774

28. Wenthold, R.J., Petralia, R.S., Blahos, J. II, and Niedzielski, A.S. (1996) Evidence for multiple AMPA receptor complexes in hippocampal CA1/CA2 neurons. *J Neurosci.***16**, 1982-1989.
29. Pei, W., Huang, Z., and Niu, L. (2007) GluR3 flip and flop: differences in channel opening kinetics. *Biochemistry* **46**, 2027-2036
30. Grunwald, M.E., and Kaplan, J.M. (2003) Mutations in the ligand-binding and pore domains control exit of glutamate receptors from the endoplasmic reticulum in C. elegans *Neuropharmacology* **45**, 768–776
31. Mah, S.J., Cornell, E., Mitchell, N.A., and Fleck, M.W. (2005) Glutamate receptor trafficking: endoplasmic reticulum quality control involves ligand binding and receptor function. *J. Neurosci.* **25**, 2215–2225
32. Valluru, L., Xu, J., Zhu, Y., Yan, S., Contractor, A., and Swanson, G.T. (2005) Ligand binding is a critical requirement for plasma membrane expression of heteromeric kainate receptors. *J. Biol. Chem.* **280**, 6085–6093
33. Vandenberghe, W., Nicoll, R.A., and Bredt, D.S. (2005) Interaction with the unfolded protein response reveals a role for stargazin in biosynthetic AMPA receptor transport. *J. Neurosci.* **25**, 1095-1102
34. Vandenberghe, W., Nicoll, R.A., and Bredt, D.S. (2005) Stargazin is an AMPA receptor auxiliary subunit. *Proc. Natl. Acad. Sci. U.S.A.* **102**, 485-490
35. Nakagawa, T. (2010) The biochemistry, ultrastructure, and subunit assembly mechanism of AMPA receptors. *Mol. Neurobiol.* **42**, 161-184
36. Mayer, M.L. (2011) Structure and mechanism of glutamate receptor ion channel assembly, activation and modulation. *Curr. Opin. Neurobiol.* **21**, 283-290.
37. Sukumaran M, Penn AC, Greger IH. (2012) AMPA receptor assembly: atomic determinants and built-in modulators. *Adv. Exp. Med. Biol.* **970**, 241-264
38. Gan, Q., Salussolia, C.L., and Wollmuth, L.P. (2015) Assembly of AMPA receptors: mechanisms and regulation. *J. Physiol.* **593**, 39-48
39. Balasuriya, D., Goetze, T.A., Barrera, N.P., Stewart, A.P., Suzuki, Y., and Edwardson, J.M. (2013) α-Amino-3-hydroxy-5-methyl-4-isoxazole propionic acid (AMPA) and N-methyl-D-aspartate (NMDA) receptors adopt different subunit arrangements. *J. Biol. Chem.* **288**, 21987-21998.
40. Zhao, H., Berger, A.J., Brown, P.H., Kumar ,J., Balbo, A., May, C.A., Casillas, E. Jr, Laue, T.M., Patterson, G.H., Mayer, M.L., and Schuck, P. (2012) Analysis of high-affinity assembly for AMPA receptor amino-terminal domains. *J. Gen. Physiol.* **139**, 371-388.
41. Kuusinen, A., Arvola, M., and Keinänen, K. (1995) Molecular dissection of the agonist binding site of an AMPA receptor. *EMBO J.* **14**, 6327–6332

**FOOTNOTES**

This work was supported by grants from the Academy of Finland (#137596; to K.K.) and from Magnus Ehrnrooth Foundation (to S.K.C, A.S. and T.M).

[§]The current address of Y.H. is Room 11-1-602, Fuyuanli community, Yizhuang, 100176 Beijing, P. R. China (Y.H.); the current address of M.W. is Forschungslabore der Frauenklinik Universitätsklinikum, Life Science Center, 40225 Düsseldorf, Germany.

The abbreviations used are: AMPA, α-amino-3-hydroxy-5-methyl-4-isoxazolepropionic acid; LBD, ligand-binding domain; NTD, N-terminal domain; ER, endoplasmic reticulum.

**FIGURE LEGENDS**

**Figure 1. GluA2 subunit rescues surface expression of GluA3.** ***(A)*** AMPA subunits GluA2-flip (GluA2i) and GluA3-flip (GluA3i) were either N-terminally Flag-tagged or C-terminally GFP-tagged and expressed in HEK293 cells, as indicated above the panels. Cells were surface biotinylated and cell extracts subjected to streptavidin pulldown (surface). Immunoblots were probed with anti-GFP. Endogenous

GAPDH protein used as a loading control. The presence of C-terminal GFP did not alter the surface trafficking phenotypes of GluA2 and GluA3. ***(B)*** GluA3i-GFP was co-expressed with GluA3i, GluA2i, GluA2-flop (GluA2o) or with the A451Y/G458R double mutant of GluA2-flip or -flop as indicated and subjected to biotinylation assay as above. Antibodies used for blotting are indicated on the right. Note that anti-GluA2/3 recognizes both GluA2 and GluA3 C-termini, but has weaker binding to GluA3. ***(C)*** Quantification of GluA3-GFP cell surface expression following co-expression with indicated proteins. Anti-GFP IgG immunoblot signals were normalized to the co-expressed GluA3i. Bars show mean ± SEM, n=7-14. Statistical analysis of the co-expressed GluA3i-GFP surface expression was determined by one-way ANOVA, $p=0.006$; Bonferroni's multiple comparison post-test gave the following p values: F-A3i vs. F-A2i, $p<0.01$ and F-A2i vs. F-A2(AG/YR) $p<0.05$, all others $p>0.05$. Dunnett's multiple comparison post test gave the following p values: F-A3i vs. F-A2i, $p<0.01$ and F-A3i vs. F-A2o, $p<0.05$, all others $p>0.05$. ***(D)*** AMPA receptor subunits GluA2i and GluA3i were N-terminally Flag (F) or Myc (M) -tagged and co-expressed in HEK293 cells, as indicated above the panels. Receptors were immunoprecipitated (IP) with either anti-Flag or anti-myc antibodies and immunoblotted as indicated below.

**Figure 2. Stargazin interacts with GluA3 but does not promote its transport to cell surface.** ***(A)*** Immunoblot of biotinylated surface GluA3 receptors expressed alone or with stargazin as detected by anti-GluA2/3 IgG (upper panel). The presence or absence of stargazin is shown in the middle panel, blotted with anti-stargazin serum. Lower panel shows endogenous GAPDH protein as a loading control. (B) Quantification of GluA3i ± stargazin surface expression immunoblots; GluA3i + stargazin signal was normalized to GluA3 expression alone. Bars show mean ± SEM, n=6. Statistical analysis by paired, one-tailed t-test gave $p=0.0762$ indicating no significant statistical difference. ***(C)*** Immunoblot showing association between GluA2i or GluA3i and stargazin. Expressed AMPA receptors were immunopreciptiated by anti-Flag antibody and the immunoprecipitates were probed for the associated stargazin (lower panel). The anti-stargazin signal ratio GluA3i+Stg/GluA2i+Stg was 1.23±0.239 (SEM), n=7. One sample t-test with control value set to one gave $p=0.38$, indicating no statistically significant difference. ***(D)*** Summed electrophysiology data from whole-cell patch-clamp recordings of HEK293 cells expressing GluA3i either alone (n=8) or with stargazin (n=9) and following application of 10 mM L-glutamate. The bars show mean ± SEM for whole-cell peak currents. Statistical analysis by unpaired one-tailed t-test gave $p=0.0764$ indicating no significant difference. ***(E)*** Comparison of tau of desensitization values from whole-cell patch-clamp recordings of HEK293 expressing either GluA3 alone (n=5) or with stargazin (n=8). Bars indicate mean ± SEM. Statistical analysis by unpaired one-tailed t-test gave $p=0.0004$, indicating stargazin has a significant effect on the desensitization kinetics of GluA3 channels.

**Figure 3. Ligand binding domain secretion mimics the cognate full-length receptor trafficking phenotype**

***(A)*** Schematic structure of the mature GluA3i LBD polypeptide expressed in mammalian cells. The included S1 and S2 residues are indicated, as are the point mutation sites; the S1 and S2 domains are joined by a flexible 13 residue linker with the sequence STEGEVNAEEEGF (13, 41). For efficient secretion, the expression plasmid encoded a viral signal peptide (MTILCWLALLSTLTAVNA) placed N-terminally from the Flag epitope (41). The numbering is from rat GluA3, Uniprot sequence P19492 (12). All LBD constructs for mammalian expression encode an N-terminal Flag tag and C-terminal Myc tag. ***(B)*** Representative immunoblots showing expression of GluA2i and GluA3i LBD proteins from transfected HEK293 cells, both 'wild-type' and point-mutated versions (upper panels, anti-Myc IgG). Left-hand panels show protein expression in cell extracts; right-hand panel shows expression of constructs in cell media following secretion. Endogenous GAPDH protein is shown as a loading control. ***(C)*** Quantitation of LBD constructs expression from cell extract (solid shading) and media (hatched shading). Immunoblot signals were normalized to GluA2 LBD expression. Bars show mean ± SEM, n=4-11. For cell extract samples one-way ANOVA gave $p=0.0006$ and for media samples one-way ANOVA $p<0.0001$. Significance determined by Dunnett's multiple comparison to GluA2i LBD as control is shown, ** indicates $p<0.01$.

**Figure 4. Instability of the LBD does not explain the poor trafficking of GluA3**
***(A)*** Schematic structure of the GluA3i LBD polypeptide expressed intracellularly in bacterial cells. The included S1 and S2 residues are indicated, as are point mutation sites; the S1 and S2 domains are joined by a two amino acid linker. All LBD constructs for bacterial expression have a C-terminal 6xHis tag for purification. ***(B)*** Typical graphs for urea denaturation of purified GluA2i and GluA3i LBD proteins following expression and purification from bacteria. Measurement was by intrinsic fluorescence spectroscopy and LBDs were denatured in absence or presence of 10 mM L-glutamate. ***(C)*** A scatter plot of measured $EC_{50}$ values for urea denaturation of GluA2i and GluA3i LBDs with or without ligand. Points indicate individual values and line is mean. Statistical analysis by one-way ANOVA gave $p<0.0001$. Bonferroni's multiple comparison test indicated a significance effect ($p<0.001$) for the presence of L-glutamate for both LBDs; it also indicated GluA3i LBD was significantly more stable than A2i LBD both without L-Glu ($p<0.05$) and with L-Glu ($p<0.01$). ***(D)*** Best fit non-linear plots of thermal denaturation of purified GluA2i, A3i and A3i(YR/AG) LBD proteins. Measurement was by CD spectroscopy. LBDs with or without L-glutamate. GluA2i is shown in blue, GluA3i in red, and A3i(YR/AG) in grey. Statistical analysis by paired t test of measured $T_m$ in the presence or absence of L-Glu indicates a significantly stabilizing effect of glutamate ($p= 0.0038$). In the absence of L-glutamate symbols and lines are solid; with L-glutamate symbols and lines are open or dashed respectively.

**Figure 5. GluA3 is more resistant to solubilization than GluA2**
***(A)*** Typical immunoblot of full length N-terminally Flag-tagged GluA2i and GluA3i expressed in HEK293 cells and following 1% Triton X-100 extraction and ultracentrifugation; soluble refers to supernatant sample and insoluble to the resultant pellet. The blot was probed with anti-Flag antibody. ***(B)*** Quantification of signal measured from such immunoblots, adjusted for the difference in final sample volume and expressed as the percentage of soluble receptor. Bars show mean ± SEM for n=13 independent experiments. Statistical analysis by paired, one-tailed student t-test gave a $p=0.0004$. ***(C)*** Immunoblot showing increased sequestering of NMDA receptor GluN1 (N1) subunit in insoluble fraction when co-expressed with GluA3i in HEK293 cells. ***(D)*** Quantification of GluN1 signal from such immunoblots and expressed as ratio GluN1+A3i/GluN1+GFP for both soluble and insoluble fraction. Bars show mean ± SEM for n=3 independent experiments. Analysis by one sample t-test with control value set to one gave $p=0.127$ for soluble fraction and $p=0.012$ for insoluble fraction. (***E***) Typical immunoblot of N-terminal Flag-tagged GluA2i and GluA3i and respective mutants expressed in HEK293 cells and following 1% Triton X-100 extraction and ultracentrifugation. Upper panel shows receptor signal from soluble fraction and the lower panel shows GAPDH loading control from the same blot. ***(F)*** Quantification of signal measured from such immunoblots and expressed as a ratio of soluble receptor to GAPDH. Bars show mean ± SEM for n=4 independent experiments. (***G***) Typical immunoblot of N-terminal Flag-tagged GluA2o and GluA3o and respective mutants expressed in HEK293 cells and following 1% Triton X-100 extraction and ultracentrifugation. Upper panel shows receptor signal from soluble fraction and the lower panel shows GAPDH loading control from the same blot. (***H***) Quantification of signal measured from such immunoblots and expressed as a ratio of soluble receptor to GAPDH. Bars show mean ± SEM for n=4 independent experiments. For both F and G, statistical analysis by one way ANOVA gave an overall $p<0.0001$, Dunnett's comparison to control (GluA3) gave: A3 vs A2, $p<0.01$; A3 vs A2(AG/YR), $p>0.05$; A3 vs A3(YR/AG) $p<0.01$. (***I***) Immunoblot of GRP78 of Triton X-100 –soluble extracts prepared from GluA2i or GluA3i expressing HEK293 cells, untransfected cells, or from untransfected cells with or without tunicamycin (2 μg/ml) treatment as indicated. Upper panel: anti-GRP78 signal; lower panel: anti-Flag signal. (***J***) Coimmunoprecipitation of GluA2i and GluA3i with GRP78. Anti-GRP78 and anti-Flag immunoblots are shown for the Triton X-100 extracts (input) and anti-Flag immunoprecipitates (IP) prepared from GluA2i or GluA3i expressing HEK293 cell extracts as indicated.

**Figure 6. Sucrose gradient analysis reveals assembly differences between the receptors**
***(A)*** Typical SDS-PAGE immunoblots of fractions following sucrose gradient centrifugation of Triton X-100 extracts from HEK293 cells expressing N-terminally Flag-tagged GluA3, GluA3 (YR/AG) and GluA2. Fraction 1 is densest and fraction 23 is lightest, as indicated by bar underneath. The subunit monomer signals are indicated by an arrowhead. A band at 250 kD and a higher aggregate smear is seen for all receptors; however, the fraction location and intensity varies. All blots were probed with anti-Flag antibody and the molecular weight markers are indicated. ***(B*** and ***C)*** Signal intensity profiles derived from the immunoblots shown. ***(B)*** shows the signal profile from the monomer band in each fraction, where $[Fn/\sum F1 - F24] * 100$. ***(C)*** shows the signal profile from entire detected signal (monomer, oligomer and aggregate) of each fraction. Peak 1 (P1) corresponds to fractions F5-8 and peak 2 (P2) corresponds to fractions F12-15.

**Figure 7. BN-PAGE analysis reveals oligomeric steady-state differences between the receptors**
***(A)*** Typical BN-PAGE immunoblots of every other fraction following sucrose gradient centrifugation of Triton-X 100 extracts from HEK293 cells expressing N-terminally Flag-tagged GluA3, GluA3 (YR/AG) and GluA2 (same samples as shown in SDS-PAGE immunoblots). Signals corresponding to aggregate (Ag), tetramer (T), dimer (D) and monomer (M) species are indicated. Boxes in the middle panel highlight the oligomeric state and regions used for the percentage analysis. Fraction numbers are indicated above and below, and P1 and P2 indicate the analyzed fractions from the peaks seen in the Figure 6 SDS-PAGE analysis. ***(B)*** Summary graph of the oligomeric state for each receptor. Bars correspond to mean ± SEM, n=5. Statistical analysis by two-way ANOVA gave an overall $p<0.0001$. Bonferroni's post-test comparison of oligomeric states between receptors indicated significant difference in aggregate and dimer states between GluA2 vs GluA3 ($p<0.001$ for both) and GluA2 vs A3 (YR/AG) ($p<0.01$ for both). However, the GluA3 wild-type *vs.* mutant did not show any significant difference for any oligomeric state. Notably, there was no significant difference in tetramer or monomer percentage between any of the receptors. ***(C)*** Graph highlighting the variation in dimer: tetramer ratio between the receptors. Bars correspond to mean ± SEM, n = 5. Statistical analysis by one-way ANOVA gave an overall $p = 0.0342$. Bonferroni's post-test comparison indicated significant difference in between GluA2 vs GluA3 ($p<0.05$) but not for any other comparison. (*D*) BN-PAGE immunoblots (anti-Flag) of crude Triton X-100 extracts prepared from HEK293 cells expressing Flag-tagged GluA2i, GluA3i, GluA2i(AG/YR) or GluA3i(YR/AG). Bots from two independent transfections are shown.

**Figure 8. GluA3 -containing receptor assembly and trafficking**
***(A)*** The location of GluA2 residues A451 and G458, corresponding to GluA3 Y454 and R461, in GluA2 tetramer model (Protein Data bank code 3kg2 ; Ref.10). The proximal and distal LBDs chains (relative to the two-fold axis of symmetry) are colored blue and green, respectively, and the A451 and G458 residues are shown as red van der Waals spheres. The upper models shows the LBD layer from above, whereas the lower model shows the tetramer from the side with NTD layer in light grey. Note the peripheral position of the residues in the proximal and central location in the distal LBDs. ***(B***) Simplified schematic of LBD organization in GluA3 homomers and in GluA2/3 heteromers. The proximal LBDs are shown as circles and the distal LBDs as squares. GluA3 residues Y454 and R461 are shown as black circles. GluA3 and GluA2 subunits are colored red and blue, respectively. Note that in GluA2/3 heteromers, Y454/R461 residues can face either outwards (heteromer 1) or inwards (heteromer 2). ***(C)*** Schematic of major assembly and transport pathways of homomeric GluA3 and heteromeric GluA2/3 receptors. Following tetramer assembly, the transport -competent heteromers (left) undergo maturation, leave the ER, and traffic to the plasma membrane. GluA3 homomers predominantly give rise to aggregation via molecular interactions involving the proximal LBDs and remain stuck within the ER. (***D***) The primary sequence surrounding the identified residues of interest (shown in blue and red) within the S1 domain in the four AMPA receptor subunits. Asterisks indicate identical residues; double dots strong similarity; single dot weak similarity.

**Table 1.** Stability of bacterially expressed LBD against urea-induced and thermal denaturation.

| | | GluA2 | GluA3 | GluA3(YR/AG) |
|---|---|---|---|---|
| $EC_{50}$ for urea (M) (mean ± SEM) | - L-Glu | 1.46 ± 0.17 | 2.23 ± 0.04 | N.D. |
| | + L-Glu (10 mM) | 4.05 ± 0.17 | 4.96 ± 0.13 | N.D. |
| $T_m$ (°C) (mean; 95 % confidence interval) | - L-Glu | 39.03 (38.70-39.37) | 45.26 (44.99-45.58) | 45.17 (44.83-45.51) |
| | + L-Glu (1 mM) | 51.37 (50.59-52.25) | 55.57 (54.91-56.22) | 55.48 (55.12-55.84) |

N.D. is not determined.

Figure 1

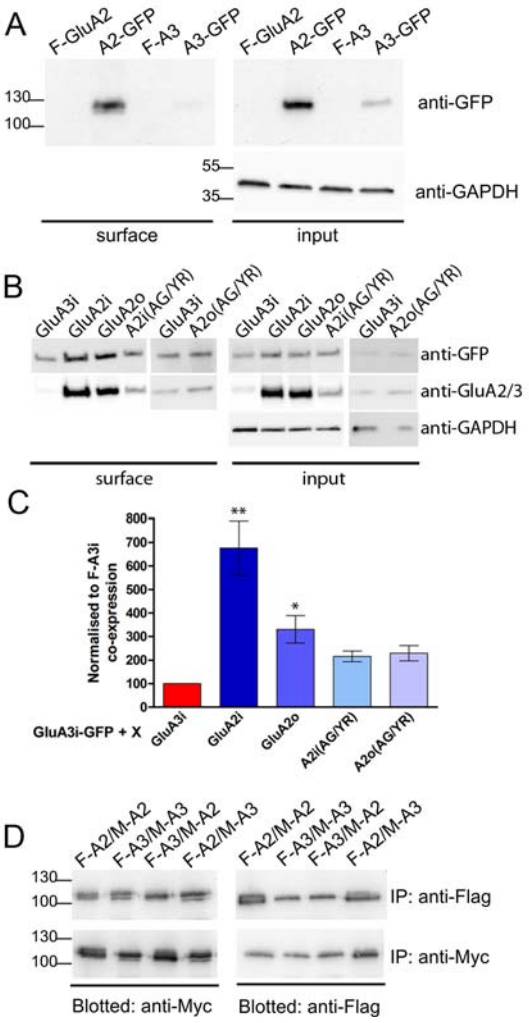
A
F-GluA2
A2-GFP
F-A3
A3-GFP
F-GluA2
A2-GFP
F-A3
A3-GFP
130
100
anti-GFP
55
35
anti-GAPDH
surface
input
B
GluA3i
GluA2i
GluA2o
A2i(AG/YR)
GluA3i
A2o(AG/YR)
GluA3i
GluA2i
GluA2o
A2i(AG/YR)
GluA3i
A2o(AG/YR)
anti-GFP
anti-GluA2/3
anti-GAPDH
surface
input
C
Normalised to F-A3i co-expression
800
700
600
500
400
300
200
100
0
**
*
GluA3i-GFP + X
GluA3i
GluA2i
GluA2o
A2i(AG/YR)
A2o(AG/YR)
D
F-A2/M-A2
F-A3/M-A3
F-A3/M-A2
F-A2/M-A3
F-A2/M-A2
F-A3/M-A3
F-A3/M-A2
F-A2/M-A3
130
100
IP: anti-Flag
130
100
IP: anti-Myc
Blotted: anti-Myc
Blotted: anti-Flag

Figure 2

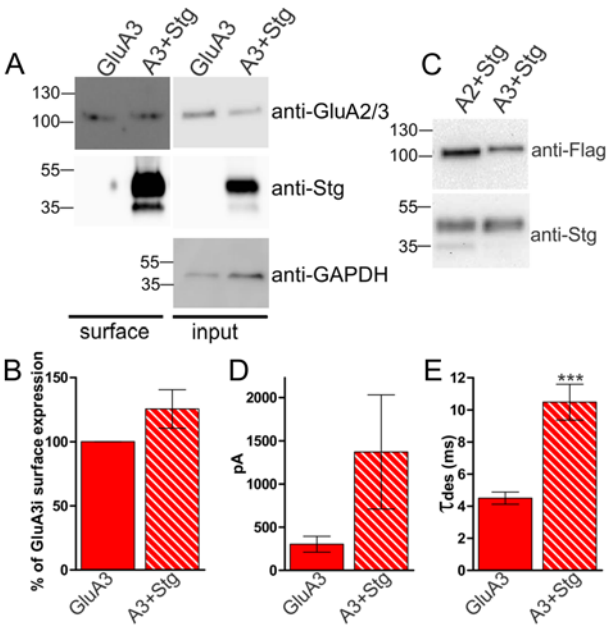
A
GluA3
A3+Stg
GluA3
A3+Stg
130
100
anti-GluA2/3
55
35
anti-Stg
55
35
anti-GAPDH
surface
input
C
A2+Stg
A3+Stg
130
100
anti-Flag
55
35
anti-Stg
B
% of GluA3i surface expression
150
100
50
0
GluA3
A3+Stg
D
pA
2000
1500
1000
500
0
GluA3
A3+Stg
E
τdes (ms)
12
10
8
6
4
2
0
***
GluA3
A3+Stg

Figure 3

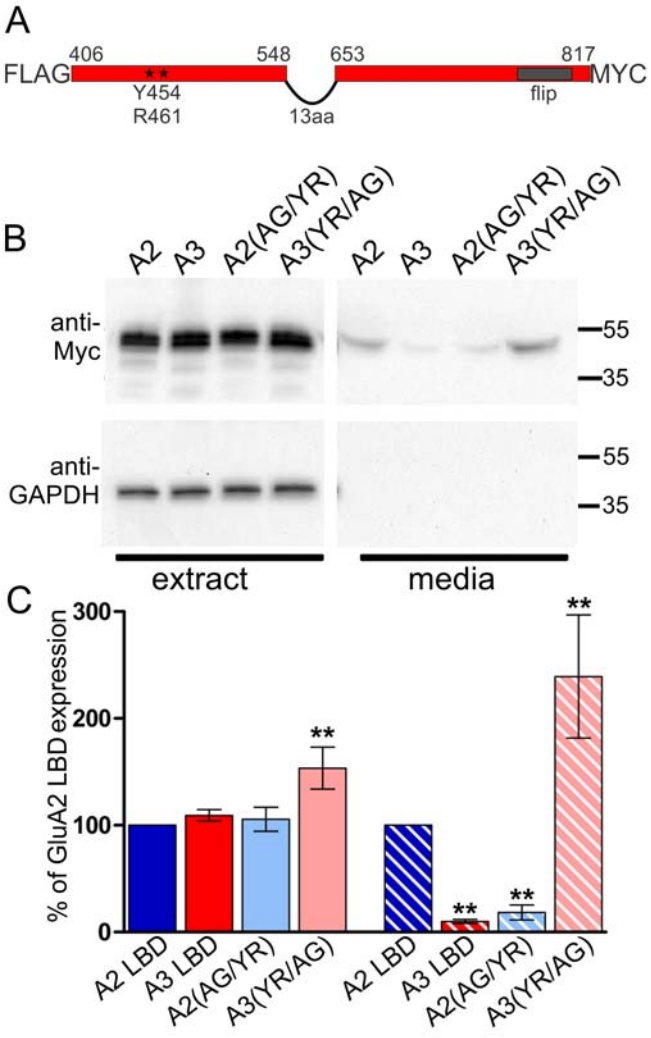
A
406
548
653
817
FLAG
MYC
Y454
R461
13aa
flip
B
A2
A3
A2(AG/YR)
A3(YR/AG)
A2
A3
A2(AG/YR)
A3(YR/AG)
anti-
Myc
55
35
anti-
GAPDH
55
35
extract
media
C
% of GluA2 LBD expression
300
200
100
0
**
**
**
**
A2 LBD
A3 LBD
A2(AG/YR)
A3(YR/AG)
A2 LBD
A3 LBD
A2(AG/YR)
A3(YR/AG)

Figure 4

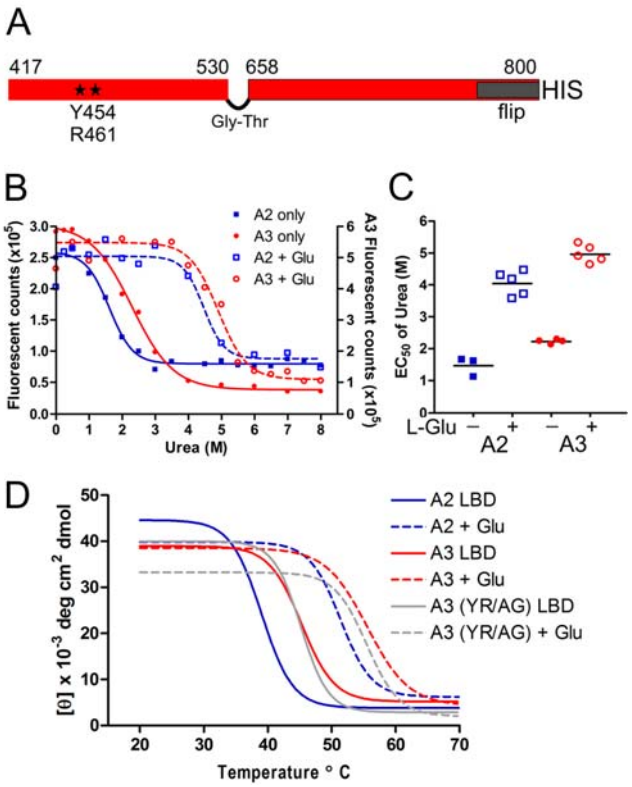
A
417
530
658
800
HIS
Y454
R461
Gly-Thr
flip
B
A2 only
A3 only
A2 + Glu
A3 + Glu
Fluorescent counts (x10^5)
A3 Fluorescent counts (x10^5)
Urea (M)
C
EC50 of Urea (M)
L-Glu
A2
A3
D
A2 LBD
A2 + Glu
A3 LBD
A3 + Glu
A3 (YR/AG) LBD
A3 (YR/AG) + Glu
[θ] x 10^-3 deg cm^2 dmol
Temperature ° C

Figure 5

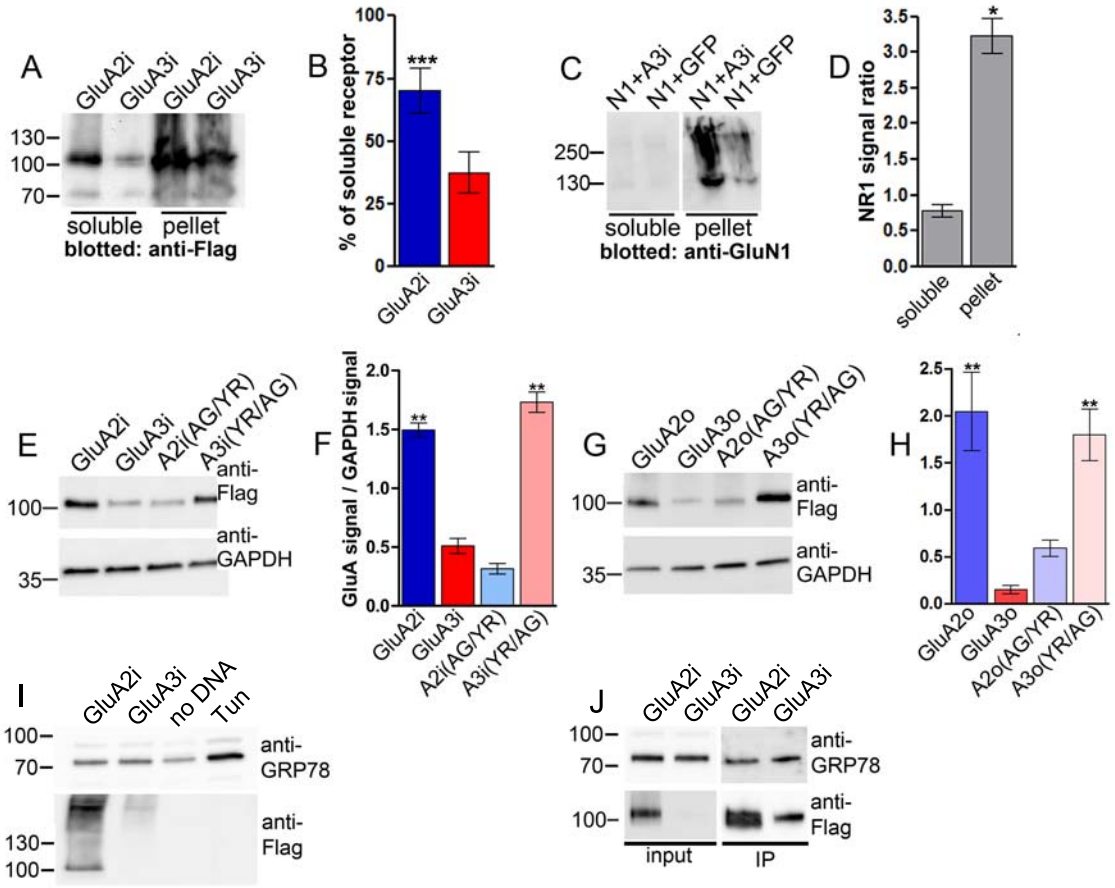
A
GluA2i
GluA3i
GluA2i
GluA3i
130
100
70
soluble
pellet
blotted: anti-Flag
B
% of soluble receptor
100
75
50
25
0
***
GluA2i
GluA3i
C
N1+A3i
N1+GFP
N1+A3i
N1+GFP
250
130
soluble
pellet
blotted: anti-GluN1
D
NR1 signal ratio
3.5
3.0
2.5
2.0
1.5
1.0
0.5
0.0
*
soluble
pellet
E
GluA2i
GluA3i
A2i(AG/YR)
A3i(YR/AG)
100
anti-Flag
35
anti-GAPDH
F
GluA signal / GAPDH signal
2.0
1.5
1.0
0.5
0.0
**
**
GluA2i
GluA3i
A2i(AG/YR)
A3i(YR/AG)
G
GluA2o
GluA3o
A2o(AG/YR)
A3o(YR/AG)
100
anti-Flag
35
anti-GAPDH
H
2.5
2.0
1.5
1.0
0.5
0.0
**
**
GluA2o
GluA3o
A2o(AG/YR)
A3o(YR/AG)
I
GluA2i
GluA3i
no DNA
Tun
100
70
anti-GRP78
130
100
anti-Flag
J
GluA2i
GluA3i
GluA2i
GluA3i
100
70
anti-GRP78
100
anti-Flag
input
IP

Figure 6

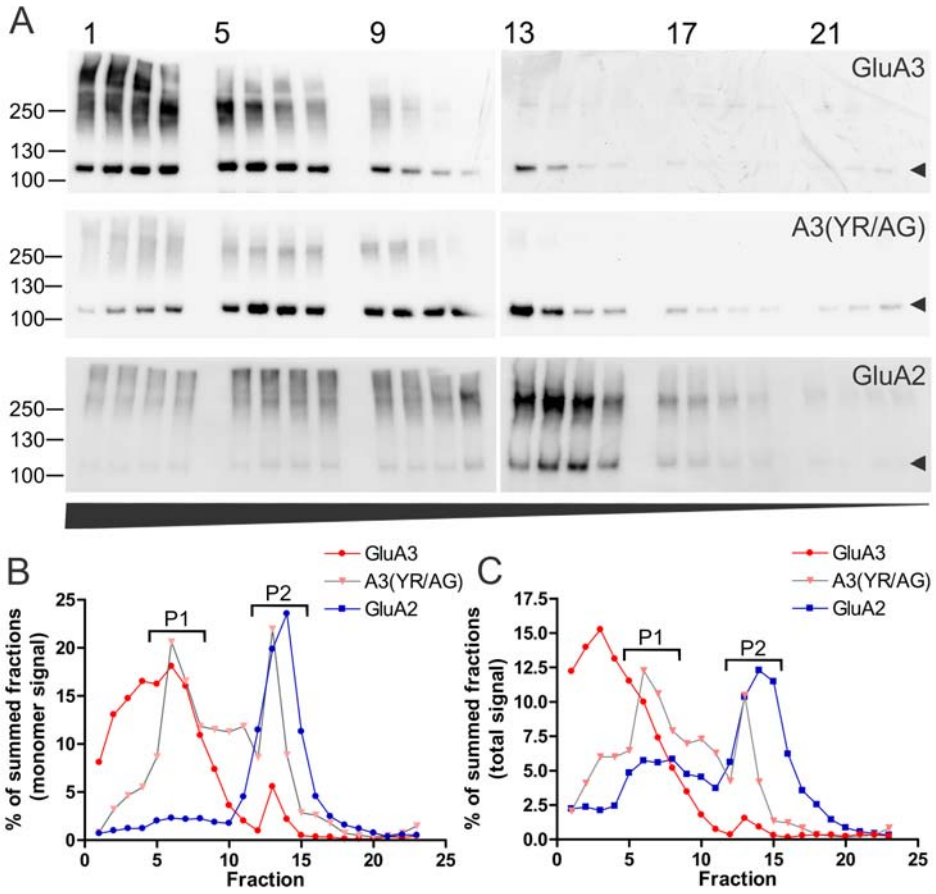
A
1
5
9
13
17
21
GluA3
A3(YR/AG)
GluA2
250
130
100
B
C
GluA3
A3(YR/AG)
GluA2
P1
P2
% of summed fractions (monomer signal)
% of summed fractions (total signal)
Fraction

Figure 7

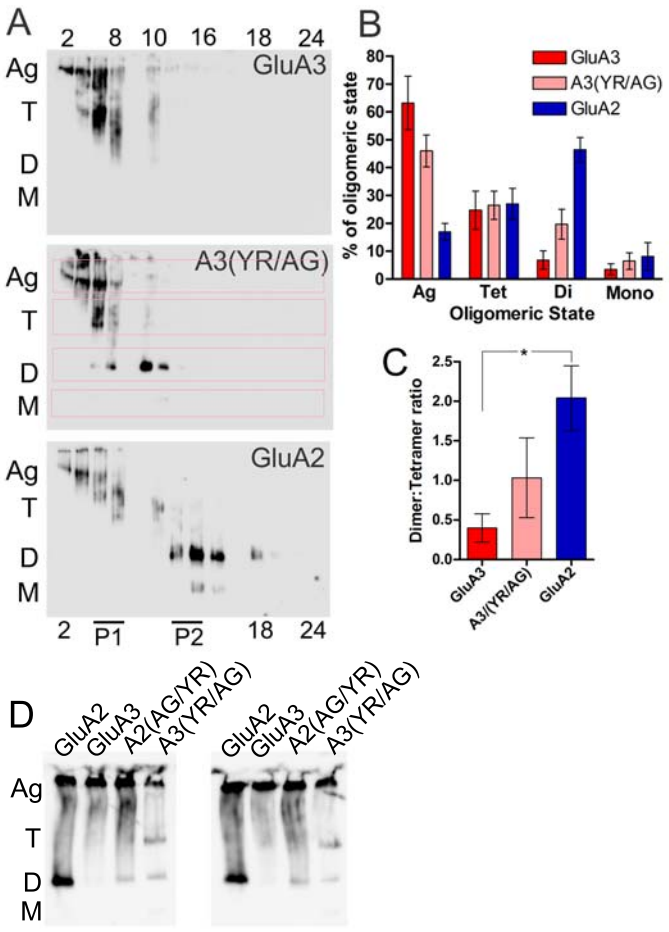
A
2 8 10 16 18 24
Ag
T
D
M
GluA3
A3(YR/AG)
GluA2
2 P1 P2 18 24
B
GluA3
A3(YR/AG)
GluA2
% of oligomeric state
Ag Tet Di Mono
Oligomeric State
C
Dimer:Tetramer ratio
GluA3
A3(YR/AG)
GluA2
D
GluA2
GluA3
A2(AG/YR)
A3(YR/AG)

Figure 8

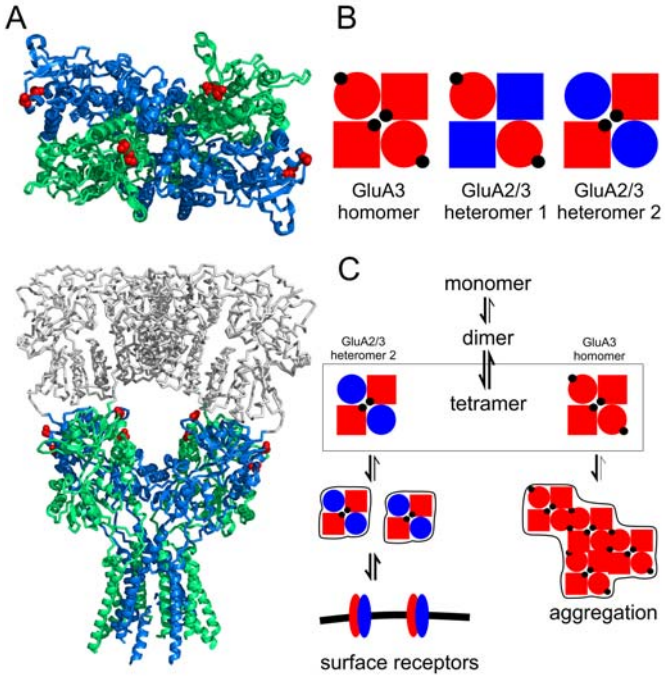


D

```
GluA1 424 KNANQFEGNDRYEGYCVELAAEIAKHVGYSYRLEIVSDGKY 464
GluA2 431 KNHEMLEGNERYEGYCVDLAAEIAKHCGFKYKLTIVGDGKY 471
GluA3 434 KNHEQLEGNERYEGYCVDLAYEIAKHVRIKYKLSIVGDGKY 474
GluA4 432 KNHEMFEGNDKYEGYCVDLASEIAKHIGIKYKIAIVPDGKY 472
          ** : :***::******:** *****   .*:: ** ****
```